ARCHIVES OF ELECTRICAL ENGINEERING VOL. 73(4), pp. 961 –976 (2024)

DOI 10.24425/aee.2024.152105

A comparative study of virtual synchronous generator and sinusoidal pulse width modulation in a wind high power conversion chain

WIJDANE EL MAATAOUI [1]✉, SOUKAINA EL DAOUDI [2], ABDELOUAHED ABOUNADA [1], MUSTAPHA MABROUKI [3]

[1] *Team of Automatic and Energy Conversion, Faculty of Sciences and Technology, Sultan Moulay Slimane University, Beni Mellal, Morocco*

[2] *Automatic, Intelligent Systems and Information Systems Team, Faculty of Sciences Semlalia, Cadi Ayyad University, Marrakech, Morocco*

[3] *Laboratory of Industrial Engineering, Faculty of Sciences and Technology, Sultan Moulay Slimane University, Beni Mellal, Morocco*

e-mail: ✉ *elmaataoui.wijdane@gmail.com*

(Received: 03.04.2024, revised: 16.11.2024)

Abstract: The virtual synchronous generator (VSG) and sinusoidal pulse width modulation (SPWM) are two prominent control strategies that have attracted particular interest recently. In this paper, we compare these two inverter control strategies in a 5MW wind power conversion chain. The studied conversion chain includes a wind turbine, a permanent magnet synchronous generator, the power converters, namely the uncontrolled rectifier, and a two-stage inverter connected to the grid via an LCL filter. Our study of the two control methods shows that both strategies reduce the total harmonic distortion (THD) while respecting the grid connection conditions. The simulation results manifest that the VSG strategy has a better THD reduction of 0.99 % which is improved compared to the SPWM with a THD of 1.33%.

Key words: maximum power point tracking (MPPT), permanent magnet synchronous generator (PMSG), sinusoidal pulse width modulation (SPWM), virtual synchronous generator (VSG), wind turbin

1. Introduction

In recent years, the transition to green energy has become a global concern. Given the exponential demand for energy and the proven harmful effects of fossil fuels, it is becoming evident that turning to renewable energy sources is the only way out [1, 2]. Among these renewable energy

sources, wind power has particularly attracted the attention of researchers. The development of wind energy conversion systems has led to a significant increase in the use of wind turbines which are considered to have a relatively low environmental impact and lower costs [3, 4].

In this paper, the considered power conversion chain consists of a wind turbine with a maximum power point tracking (MPPT) controller connected to a permanent magnet synchronous generator (PMSG). The PMSG is followed by power converters, namely the rectifier and the inverter. This inverter is controlled by the two control strategies SPWM and VSG that are the subject of our study. The power conversion chain is then connected to the grid via the LCL filter.

The MPPT is important for wind turbines, because it allows maximum wind power to be extracted under different weather conditions, optimizing wind turbine performance, and maximizing energy production [5]. MPPT techniques include, among others, tip speed ratio (TSR), power signal feedback (PSF), and optimal torque (OT) control. TSR control presents the advantage of being constant for a given wind turbine regardless of wind speed. PSF, on the other hand, is based on the optimal reference power curve of the wind turbine, which must first be obtained from experimental results, while OT maintains the system operation in λ_{opt} mode, guaranteeing the transformation of wind energy into a mechanical form [6, 7], which is why we chose to use it here.

The mechanical energy supplied by the wind turbine is converted into electrical energy via an electrical generator. The PMSG was chosen in this study for its reliability, high efficiency, gearless construction, and self-excitation characteristics. To interface the wind turbine and generator with the grid, power electronic converters are required. The output of the rectifier is always a direct current. Therefore, an inverter is needed to convert it into an alternating current. SPWM can be used to control the switching signals of the power electronic devices in the inverter. The main advantage of this switching technique is the reduction of harmonics in the inverter output signal [8, 9].

VSG control is an interesting technology for researchers interested in distributed generation systems. It adds artificial inertia to the grid, which can improve its stability and reliability. It also enables efficient control of inverters, which provide virtual inertia to ensure frequency stability [10, 11]. The advantages of VSG control are that it improves grid stability and reliability by preventing outages and reducing the risk of blackouts by stabilizing grid frequency and voltage. The VSG also has disadvantages, such as cost, complexity, and the impact on inverter performance, which can lead to a reduction in efficiency. Despite these drawbacks, the advantages of VSG control outweigh the disadvantages, as this technology improves the stability and reliability of power grids, which is important to researchers in this field [12]. Current research in VSG control focuses on improving the performance of control algorithms, reducing implementation costs, and increasing flexibility by adapting to different types of power systems and different energy sources [13].

Connecting the wind energy conversion chain to the grid requires certain conditions, including a total harmonic distortion that meets grid connection requirements. Consequently, filtering is required to suppress harmonics, and among the filter design methods that have been discussed in the literature are the L, C, LC, and LCL filters. The LCL filter is the most common choice due to its greater dynamic range compared to L, C, or LC filters, and its size, simplicity, and efficiency in reducing reactive power consumption [14, 15].

The motivation of this work is to compare two control strategies; the SPWM control with one voltage loop and two current loops against the VSG control with a double loop to generate inverter control pulses from active and reactive power. To prove the efficiency of the VSG control by comparing the active and reactive power, the total harmonic distortion (THD) of the output current,

and the phase-locked loop synchronization of both control strategies. Constraints are also used to prove the robustness of the phase-locked loop (PLL), which enables synchronization with the grid.

The rest of this paper is structured as follows: The schematic diagram of the power conversion chain, the wind turbine modeling, the state representation of the PMSG model, and the optimal torque control are presented in the second section, while the third section is dedicated to the inverter controls, namely SPWM control and VSG control. The results of the simulations for the two inverter controls are presented and discussed in the fourth section before concluding.

2. Wind energy conversion

The schematic diagram of the wind energy conversion chain illustrated in Fig. 1 consists of the wind turbine, the permanent magnet synchronous generator, the rectifier, the two-stage inverter, the LCL filter, as well as the MPPT loop, the multi-variable band-pass filter (MVBPF) block and the usual *dq*-PLL, and the inverter control loops.

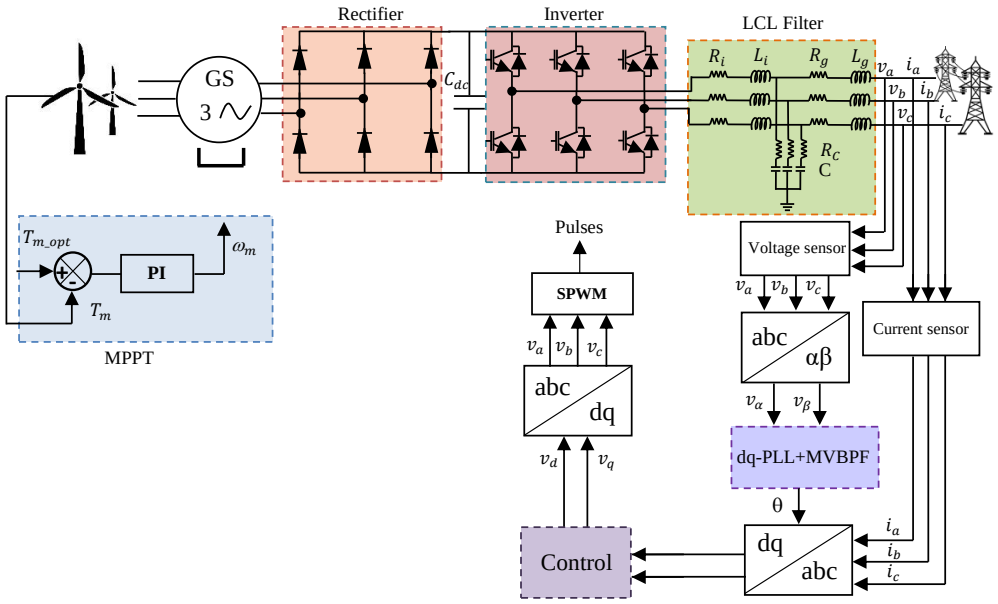

Fig. 1. Schematic illustration of the wind energy conversion chain

2.1. Wind turbine modeling

The process of converting wind energy into mechanical torque requires the use of a wind turbine. The mechanical power of the turbine, which is derived from the power of the wind, can be used to calculate this torque. The ratio between the mechanical power (P_m) and the wind power (P_w) is called the turbine power coefficient (C_p) [16].

$$C_p = \frac{P_m}{P_w} < 1. \tag{1}$$

The "Betz limit" of 0.593 is the theoretical limit of the power coefficient, which is dependent on the bank angle (β) and maximum speed (λ). In actuality, this limit is never achieved, hence the power extracted from the wind turbine is limited to 59.3% [17].

In terms of maximum speed (λ) and angle of inclination (β), the power coefficient (C_p) is also represented as follows:

$$C_p(\beta,\lambda) = (\beta-2)(0.35-0.00167)\sin\left(\frac{\pi(\lambda+0.1)}{14.34-0.3(\beta-2)}\right) - 0.00184(\lambda-3)(\beta-2). \tag{2}$$

The mechanical power equation is expressed as follows:

$$P_m = C_p(\lambda,\beta)\frac{\rho S}{2}v_{\text{wind}}^3. \tag{3}$$

The mechanical torque equation is:

$$T_m = \frac{P_m}{\omega_T}. \tag{4}$$

where: (T_m) is the mechanical torque, (P_m) is the mechanical power, (ω_T) is the turbine rotation speed, (S) is the area swept by the turbine, (λ) is the tip speed ratio, (β) is the blade pitch angle, (ρ) is the air density and (v_{wind}) is the wind speed in m/s.

2.2. State representation of the permanent magnet synchronous generator

The mathematical model of the PMSG requires the adoption of certain simplifying assumptions, as this makes it easier to study and operate [18].

In the reference frame (abc), the electrical equations of the PMSG are expressed as follows:

$$\begin{bmatrix} v_a \\ v_b \\ v_c \end{bmatrix} = -\begin{bmatrix} R_s & 0 & 0 \\ 0 & R_s & 0 \\ 0 & 0 & R_s \end{bmatrix}\begin{bmatrix} i_a \\ i_b \\ i_c \end{bmatrix} + \frac{\mathrm{d}}{\mathrm{d}t}\begin{bmatrix} \varphi_a \\ \varphi_b \\ \varphi_c \end{bmatrix}, \tag{5}$$

where: (i_a, i_b, i_c) are the stator currents, (v_a, v_b, v_c) are the stator voltages, (R_s) is the stator winding resistance, and ($\varphi_a, \varphi_b, \varphi_c$) are the stator fluxes.

After Park transformation, the following are the voltage equations:

$$\begin{cases} v_d = -R_s i_d - \dfrac{\mathrm{d}\varphi_d}{\mathrm{d}t} + \left(\dfrac{\mathrm{d}\theta}{\mathrm{d}t}\right)\varphi_q \\ v_q = -R_s i_q - \dfrac{\mathrm{d}\varphi_q}{\mathrm{d}t} - \left(\dfrac{\mathrm{d}\theta}{\mathrm{d}t}\right)\varphi_d \end{cases}. \tag{6}$$

The following are the flow expressions along the (d-q) axis:

$$\begin{cases} \varphi_d = L_d i_d + \varphi_f \\ \varphi_q = L_q i_q \end{cases}. \tag{7}$$

The direct and quadrature inductances denoted as (L_d) and (L_q), are supposed to be independent of (θ) which is the absolute position of the rotor. (φ_f) represents the magnets' flux.

The following is the expression for the voltage equations along the (d-q) axis.

$$\begin{cases} v_d = -R_s i_d - L_d \dfrac{\mathrm{d}i_d}{\mathrm{d}t} + \omega L_q i_q \\ v_q = -R_s i_q - L_q \dfrac{\mathrm{d}i_q}{\mathrm{d}t} - \omega L_d i_d - \omega \varphi_f \end{cases}. \tag{8}$$

The matrix representation of these equations is as follows:

$$\begin{bmatrix} v_d \\ v_q \end{bmatrix} = -\begin{bmatrix} R_s & 0 \\ 0 & R_s \end{bmatrix} \begin{bmatrix} i_d \\ i_q \end{bmatrix} + \begin{bmatrix} -L_d & 0 \\ 0 & -L_q \end{bmatrix} \frac{\mathrm{d}}{\mathrm{d}t} \begin{bmatrix} i_d \\ i_q \end{bmatrix} + \omega \left(\begin{bmatrix} 0 & L_q \\ -L_d & 0 \end{bmatrix} \begin{bmatrix} i_d \\ i_q \end{bmatrix} - \begin{bmatrix} 0 \\ \varphi_f \end{bmatrix} \right). \tag{9}$$

2.3. Optimal torque control (OT)

Running the system in (λ_{opt}) mode ensures that the wind energy that is accessible is transformed into mechanical form. The principle of this method, presented in Fig. 2, is to modify PMSG torque by the reference torque of maximum wind turbine power at a specific wind speed [5]. The wind turbine's output power as a function of (λ) and (ω_T) can be expressed as follows:

$$\lambda = \frac{\omega_T R}{v_{\text{wind}}}, \tag{10}$$

$$P_m = \frac{1}{2} \rho \pi R^5 C_p \frac{\omega_T^3}{\lambda^3}, \tag{11}$$

where (ω_T) is the turbine rotation speed and (R) is the blade radius.

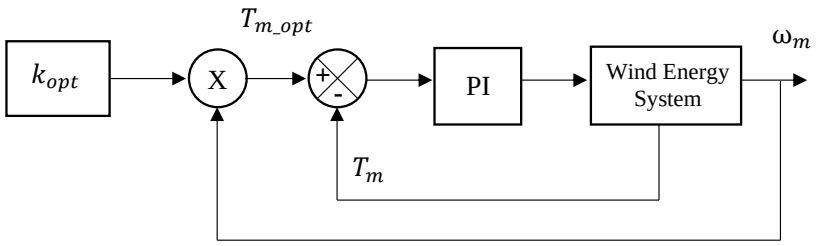

Fig. 2. Schematic diagram of the MPPT method for optimal torque control

If the rotor turns at (λ_{opt}), it will also operate on ($C_{P\,\max}$). The power expression will then be:

$$P_{m\text{-opt}} = \frac{1}{2} \rho \pi R^5 \frac{C_{P\,\max}}{\lambda_{\text{opt}}^3} \omega_T^3. \tag{12}$$

Considering

$$k_{\text{opt}} = \frac{1}{2} \rho \pi R^5 \frac{C_{P\,\max}}{\lambda_{\text{opt}}^3}, \tag{13}$$

then

$$T_{m-\text{opt}} = k_{\text{opt}} \omega_T^2. \tag{14}$$

This is a method based on torque control, where the reference torque for the controller attached to the wind turbine is determined by the analytical expression of the optimal torque curve. This approach is generally easy to use, quick, and effective.

3. Inverter controls

3.1. Voltage and current control

This control is made up of two cascaded loops which are the voltage regulation loop in the first place and the current regulation loop in the second [19, 20]. This control technique is illustrated in Fig. 3 with the other blocks of the wind turbine power conversion chain.

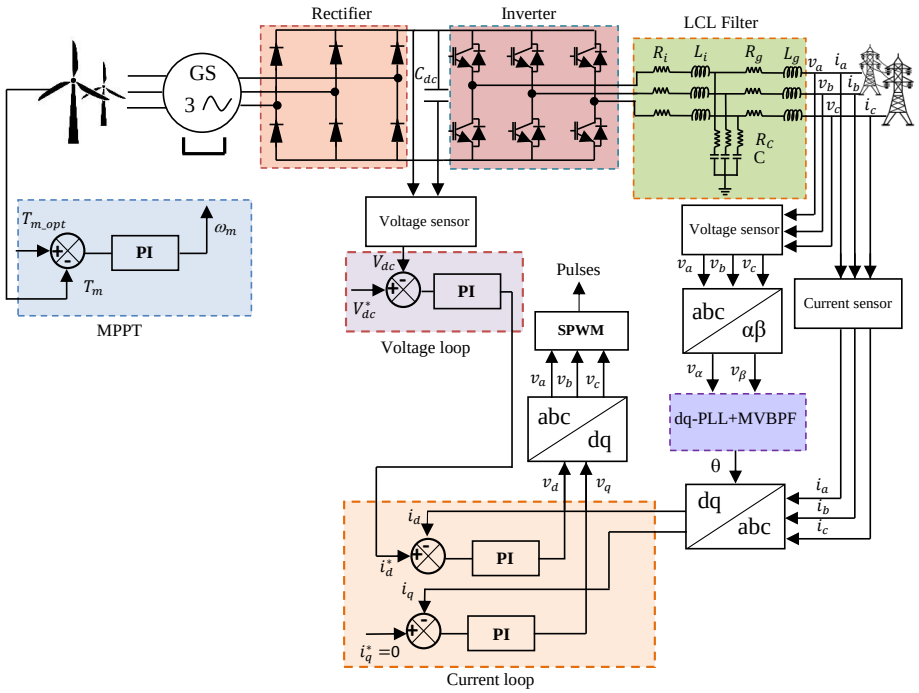

Fig. 3. Schematic illustration of the wind energy conversion chain with voltage and current control

Current regulation

The current regulation loop represented in Fig. 4 comprises a PI regulator with four other blocks, namely the control, inverter, filter, and sampling block.

The following is the expression for the PI controller's transfer function:

$$F_{\mathrm{PI}}(s) = \frac{sk_p + k_i}{s}. \tag{15}$$

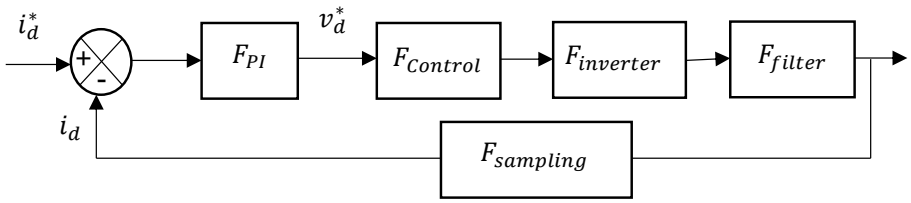

Fig. 4. Current regulation loop

The control's transfer function is expressed as a 1st order system:

$$F_c(s) = \frac{1}{sT_{sa} + 1}, \tag{16}$$

where $T_{sa} = \frac{1}{f_{sa}}$ is the sampling period.

The following is the expression for the inverter's transfer function:

$$F_{\text{inv}}(s) = \frac{1}{sT_s + 1}, \tag{17}$$

where (T_s) is the period of switching.

The LCL filter's transfer function is as follows:

$$F_{\text{filter}}(s) = \frac{K_{eq}}{1 + sT_{eq}}, \tag{18}$$

with $K_{eq} = \dfrac{1}{R_i + R_g}$ and $T_{eq} = \dfrac{L_i + L_g}{R_i + R_g}$.

The sampling delay can be expressed as follows:

$$F_{\text{sampling}} = \frac{1}{1 + \dfrac{S}{2}T_{sa}}. \tag{19}$$

The following is the expression of the closed loop current control's transfer function:

$$F_{c,BF} = \frac{\dfrac{K_{eq}}{T_{eq}\left(k_i + sk_p\right)}}{s^2 + \dfrac{1 + K_{eq}k_p}{T_{eq}}s + \dfrac{K_{eq}k_i}{T_{eq}}}. \tag{20}$$

Once the closed-loop transfer function has been determined using a second-order system, the expressions for the PI controller parameters are written as follows:

$$\begin{cases} k_i = (L_i + L_g)\omega_n^2 \\ k_p = 2\xi\omega_n(L_i + L_g) - (R_i + R_g) \end{cases}, \tag{21}$$

where (ξ) is the damping factor, and (ω_n) is the nominal pulsation.

Voltage regulation

The reference current at the output along the d-axis is provided by the voltage regulation loop shown in Fig. 5. It is composed of a PI regulator, the current regulation transfer function, and the voltage dynamics equation.

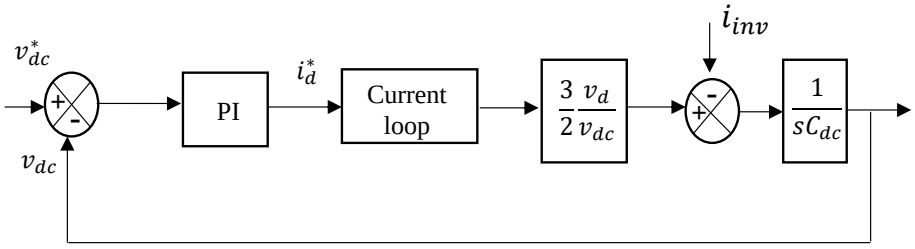

Fig. 5. Voltage regulation loop

The DC voltage's dynamic equation is expressed as follows:

$$\frac{3}{2}\frac{v_d}{v_{dc}}i_d - i_{\text{inv}} = C_{dc}\frac{\mathrm{d}v_{dc}}{\mathrm{d}t}. \tag{22}$$

The DC link voltage is represented by (v_{dc}), the DC link capacitance by (C_{dc}), and the grid-side voltages along the d-q axis by (v_d) and (v_q).

The following is the written expression for the current control's closed-loop transfer function:

$$F_{c,BF} = \frac{1 + T_{sa}}{1 + 4sT_{sa}}. \tag{23}$$

where (T_{sa}) is the sampling time.

The expression for the open-loop DC voltage transfer function can be expressed as follows:

$$H_{dc,BO} = \frac{3}{2}k_p\left(\frac{1 + sT_i}{sT_i}\right)\left(\frac{1}{s \times 4T_{sa} + 1}\right)\left(\frac{v_d}{sC_{dc}v_{dc}}\right). \tag{24}$$

To apply the optimum symmetry criterion, the expression of the PI controller parameters is as follows:

$$\begin{cases} k_p = \dfrac{C_{dc}}{18T_{sa}} \\ k_i = \dfrac{C_{dc}}{648T_{sa}^2} \end{cases}. \tag{25}$$

3.2. Virtual synchronous generator control

This technique, shown in Fig. 6, simulates the mechanical and electromagnetic characteristics and regulates the grid-connected inverter to control the synchronous generator's rotation and damping properties. The VSG also synchronizes frequency and phase with the grid and generates inverter control pulses from the dual loop and the active and reactive power loops [21, 22].

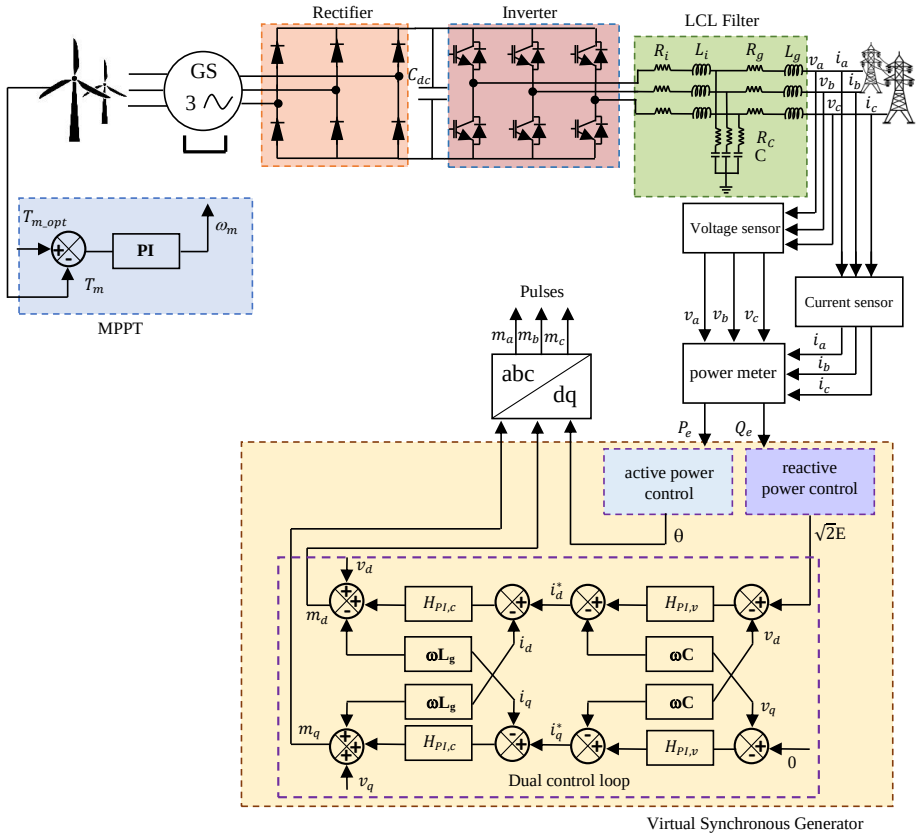

Fig. 6. Schematic diagram of wind energy conversion chain with VSG control system

Active power control design

Applying the fundamental principle of dynamics to a rotating mass, the swing equation is as follows:

$$J\alpha_m = \sum T_i = T_m - T_e, \tag{26}$$

where: (T_e) is the electrical torque, (T_m) is the mechanical torque, (J) is the total inertia moment and (α_m) is the angular acceleration of the rotor.

Then the swing equation becomes [23]:

$$J\omega_m \frac{\mathrm{d}\omega_m}{\mathrm{d}t} = P_m - P_e. \tag{27}$$

To represent the dampers of the synchronous machine, a damping term is added, so that:

$$J\omega_m \frac{\mathrm{d}\omega_m}{\mathrm{d}t} = P_m - P_e - D_p(\omega_m - \omega_{\mathrm{ref}}), \tag{28}$$

where: (D_p) is the damping factor, (ω_{ref}) is the reference angular speed, and (ω_m) is the rotation speed. (P_m) and (P_e) are, respectively, the active mechanical and electrical output power.

Reactive power control design

This type of control improves voltage stability and prevents excessive current flow in the network. The inverter neutral point voltage control equation is given by the following expression [24]:

$$\sqrt{2}E_{\text{ph}} = G(s)\left(\sqrt{2}U_{\text{ref}} - \sqrt{2}U_n\right), \tag{29}$$

where (E_{ph}) is the phase voltage of the inverter, and (U_{ref}) is the inverter reference voltage. (U_n) is the inverter's real output voltage, by the reactive power-voltage Q-V droop equation, is comparable to the basic voltage regulation function:

$$D_q\sqrt{2}\,(U_n - U_{\text{ref}}) = Q_e - Q_{\text{ref}}. \tag{30}$$

(U_n) is the nominal output voltage that must be matched to the electrical network. (Q_e) and (Q_{ref}) are the real output reactive power of the converter and the reference reactive power setting, respectively, and (D_q) is the reactive power and voltage droop coefficient.

According to the two previous equations:

$$\sqrt{2}E_{\text{ph}} = \frac{H(s)}{D_q}\left(Q_e - Q_{\text{ref}} + D_q\left(\sqrt{2}U_n - \sqrt{2}U_{\text{ref}}\right)\right). \tag{31}$$

By taking $(H(s) = D_q/k_i s)$, where (k_i) is the integral gain, the Q-V equation is expressed as follows:

$$\sqrt{2}E_{\text{ph}} = \frac{1}{k_i s}\left(Q_e - Q_{\text{ref}} + D_q\left(\sqrt{2}U_n - \sqrt{2}U_{\text{ref}}\right)\right). \tag{32}$$

Voltage and current loops

The traditional VSG cannot control the voltage output. Therefore, an internal current loop and an external voltage loop in a double closed-loop control structure is usually added to further improve voltage and current outputs.

– Voltage control

The inverter's DC intermediate circuit is represented by [25]:

$$i = C_{\text{DC}}\frac{\mathrm{d}v}{\mathrm{d}t} + i_{\text{inv}}. \tag{33}$$

Assuming that the rotary marker's d-axis is parallel to the AC network voltage, v_q^* is equal to zero:

$$\begin{bmatrix} i_d^* \\ i_q^* \end{bmatrix} = \left(\frac{1}{R_C} + \frac{C_{\text{DC}}}{s}\right)\begin{bmatrix} v_d^* - v_d \\ v_q^* - v_q \end{bmatrix} - C\omega\begin{bmatrix} v_d \\ v_q \end{bmatrix}. \tag{34}$$

The transfer function of the PI controller is as follows:

$$H_{\text{PI}} = k_p + \frac{k_i}{s}.$$

By identification with Eq. (34), $k_p = \dfrac{1}{R_C}$ and $k_i = C_{\text{DC}}$.

(v_d), (v_q), (i_d^*), and (i_q^*) in Eq. (34) are the output voltage and current's d- and q-axis components, respectively. (C) is the filter capacitor, as well as (v_d^*) and (v_q^*), the d- and q-axes, respectively, correspond to the DC bus reference voltage components.

– Current control
The grid-side conversion chain consists of a DC bus represented by a capacitor, the grid-coupled filter, and the three-phase inverter, which stands for the point of common coupling (PCC). The balanced voltages at the grid-side filter's terminals are expressed as follows in the d–q reference frame [26, 27]:

$$\begin{cases} m_d = \left(R_g + \dfrac{L_g}{s}\right)(i_d^* - i_d) - \omega L_g i_q + v_d \\ m_q = \left(R_g + \dfrac{L_g}{s}\right)(i_d^* - i_d) + \omega L_g i_d + v_d \end{cases}. \tag{35}$$

By identification with Eq. (35), $k_p = R_g$ and $k_i = L_g$.

(L_g) and (R_g) in Eq. (35) are the filter's network-side inductance and resistance, and (ω) is the network voltage's angular frequency. The d- and q-axis components of the common coupling point voltage are denoted by (v_d) and (v_q), respectively. The current loop's d- and q-axis output reference values are denoted by (m_d) and (m_q). (i_d), (i_q), (i_d^*), and (i_q^*) show the components of the d- and q-axes of the network-side currents and the output reference currents of the voltage loop, respectively.

4. Simulations

The simulations of the two systems presented in this paper are performed using MATLAB/SIMULINK software. To prove the efficiency of the closed-loop wind energy conversion chain, two simulations are carried out; the first concerns the wind energy conversion chain with SPWM control, and the second simulation with VSG control. The robustness of the PLL synchronization loop is also simulated.

In Fig. 7 we compare the total harmonic distortion (THD) of the output current of the two control strategies SPWM and VSG. Figure 7(b) shows the spectrum analysis of the output current

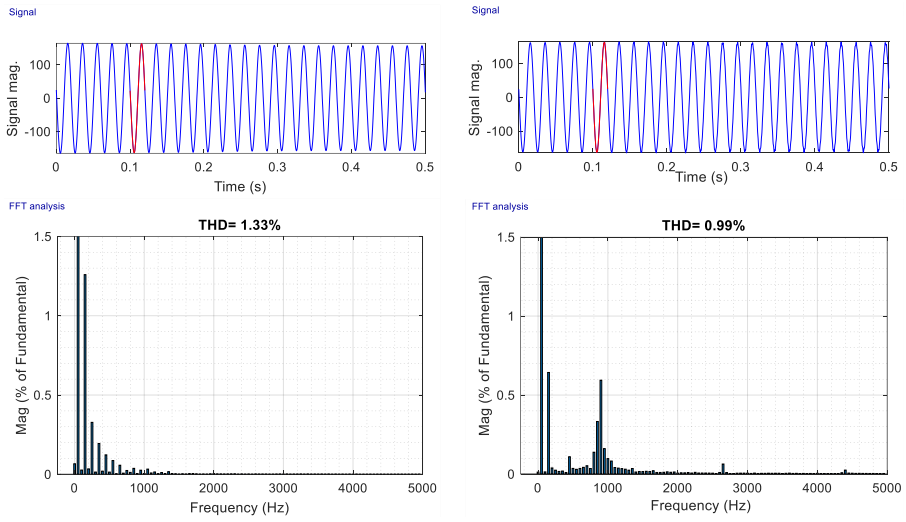

(a) (b)

Fig. 7. Output current total harmonic distortion with SPWM control (a) and VSG control (b)

of the VSG control combined with the optimized LCL filter in the wind energy conversion chain. The total harmonic distortion in this case is well reduced by 0.99% compared to the previous structure with SPWM control, which has a total harmonic distortion of 1.33% (Fig. 7(a)). The VSG control shows a better THD reduction compared to the SPWM control, and considering the grid connection conditions, we can also notice that the third-order harmonics are much reduced for the VSG control compared to the SPWM control, which explains the efficiency of this method.

In Fig. 8 we compare the active power supplied to the grid for the wind energy conversion chain with two control strategies namely SMPW and VSG. From the comparison of the two figures, the active power is more stable with the VSG control. These simulation results show the robustness of the VSG control strategy considering the grid connection conditions.

Figure 9 shows a comparison of the reactive power with both control methods, the SPWM and the VSG. The simulation results show that the reactive power remains at zero with a small transient regime. This demonstrates the reliability of the methods.

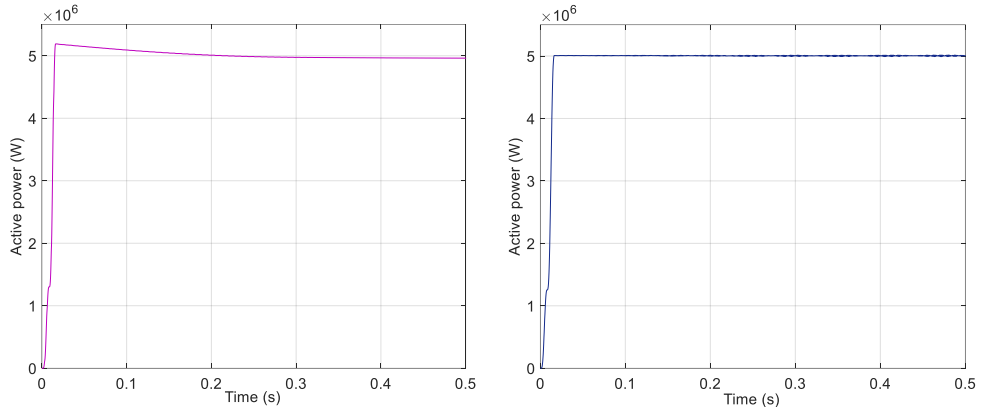

Fig. 8. Active power with SPWM control (a) and VSG control (b)

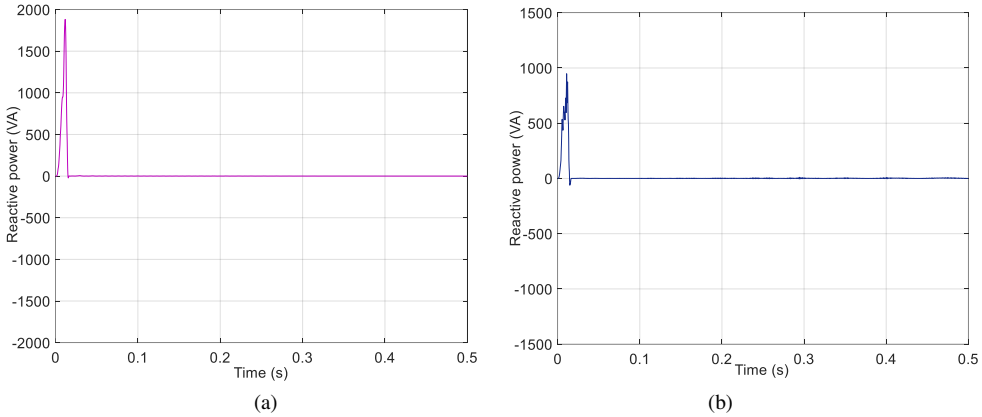

Fig. 9. Reactive power with SPWM control (a) and VSG control (b)

In Fig. 10 we compare the theta angle at the output of the PLL synchronization loop without perturbation and with white noise perturbation. By applying a white noise perturbation to the input of the PLL synchronization loop, the theta angle (θ) at the output of the loop remains stable. The comparison of the two diagrams demonstrates the robustness of the synchronization loop.

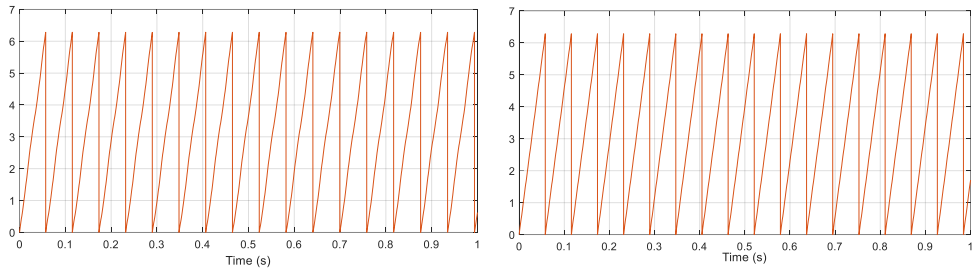

(a) (b)

Fig. 10. Theta angle at the output of the PLL synchronization loop without perturbation (a) and with white noise perturbation (b)

Table 1 shows the parameters of the systems studied previously, Table 2 shows the parameters of the filter dimensioned for 5 MW active power, and Table 3 shows the parameters of the PI controllers studied in this paper, namely optimal torque control, voltage control, and current control.

Table 1. System specifications

Parameter name	**Symbol**	**Value**	**Unit**
Active power	P	5	MW
Reactive power	Q	0	VA
Network frequency	f	50	Hz
Phase voltage	E_{ph}	$2{,}5.10^4$	V
Switching frequency	f_{sw}	10	kHz

Table 2. Parameters of the filter

Parameter name	**Symbol**	**Value**	**Unit**
Resistance on the inverter side	R_i	4 373.03	Ω
Inductance on the inverter side	L_i	0.033	H
Damping resistance	R_C	217.97	Ω
Filter capacity	C	$8\ 544.10^{-3}$	F
Resistance on the grid side	R_g	174.93	Ω
Inductance on the grid side	L_g	$5\ 676.10^{-6}$	H

Table 3. PI controller parameters

Parameter name		Symbol	Value
Optimal torque control		k_p	211.10^{-3}
		k_i	448.10^{-3}
Voltage control		k_p	611.10^{-5}
		k_i	848.10^{-7}
Current control		k_p	0.074
		k_i	0,07
Dual control loop	Voltage control	k_p	$4\ 587.10^{-3}$
		k_i	$2\ 200.10^{-6}$
	Current control	k_p	$174\ 930.10^{-2}$
		k_i	$5\ 676.10^{-6}$

5. Conclusion

In this paper, we presented a comparative study between two inverter control methods in a wind power conversion chain, namely Sinusoidal Pulse Width Modulation (SPWM) control and Virtual Synchronous Generator (VSG) control. Our study examined several comparative aspects, including active and reactive power, total harmonic distortion of the output current, and the output of the phase-locked-loop synchronization with and without noise perturbation. Although the two strategies showed similar and stable results for almost all of these indicators, we still find a difference when it comes to THD, with VSG showing better THD reduction of 0.99% according to our simulations compared to the SPWM with a THD of 1.33%. Using the same experimental setup, future work could investigate the use of a non-linear command of the inverter.

Acknowledgements

The authors would like to express their gratitude to the anonymous reviewers for their insightful and constructive criticism, which significantly improved the paper's final draft. Additionally, they express their gratitude to the Editors for their kind remarks and assistance.

References

[1] Dahbi A., Nait-Said N., Nait-Said M., *A novel combined MPPT-pitch angle control for wide range variable speed wind turbine based on neural network*, International Journal of Hydrogen Energy, vol. 41, iss. 22, pp. 9427–9442 (2016), DOI: 10.1016/j.ijhydene.2016.03.105.

[2] Krishnama Raju S., Pillai G.N., *Design and real time implementation of type-2 fuzzy vector control for DFIG based wind generators*, Renewable Energy, vol. 88, pp. 40–50 (2016), DOI: 10.1016/j.renene.2015.11.006.

[3] Nguyen D., Fujita G., *Analysis of sensorless MPPT method for hybrid PV-Wind system using DFIG Wind Turbines*, Sustainable Energy, Grids and Networks, vol. 5, pp. 50–57 (2016), DOI: 10.1016/j.segan.2015.11.001.

[4] Gao Z., Liu X., *An Overview on Fault Diagnosis, Prognosis and Resilient Control for Wind Turbine Systems*, Processes 9, no. 2, 300 (2021), DOI: 10.3390/pr9020300.

[5] Abdullah M.A., Yatim A.H.M., Tan C.W., Saidur R., *A review of maximum power point tracking algorithms for wind energy systems*, Renewable and Sustainable Energy Reviews, vol. 16, iss. 5, pp. 3220–3227 (2012), DOI: 10.1016/j.rser.2012.02.016.

[6] Yin M., Li W., Chung C.Y., Zhou L., Chen Z., Zou Y., *Optimal torque control based on effective tracking range for maximum power point tracking of wind turbines under varying wind conditions*, Iet Renewable Power Generation, vol. 11, no. 4, pp. 501–510 (2017), DOI: 10.1049/iet-rpg.2016.0635.

[7] Meghni B., Chojaa H., Boulmaiz A., *An Optimal Torque Control based on Intelligent Tracking Range (MPPT-OTC-ANN) for Permanent Magnet Direct Drive WECS*, IEEE 2nd International Conference on Electronics, Control, Optimization and Computer Science (ICECOCS), Kenitra, Morocco, pp. 1–6 (2020), DOI: 10.1109/ICECOCS50124.2020.9314304.

[8] Abdolrasol M.G., Hannan M., Hussain S.S., Ustun T.S., *Optimal PI controller based PSO optimization for PV inverter using SPWM techniques*, Energy Reports, vol. 8, supplement 1, pp. 1003–1011 (2022), DOI: 10.1016/j.egyr.2021.11.180.

[9] Sarker R., Datta A., Debnath S., *FPGA-based variable modulation-indexed-SPWM generator architecture for constant-output-voltage inverter applications*, Microprocessors and Microsystems, vol. 77, 103123 (2020), DOI: 10.1016/j.micpro.2020.103123.

[10] Bao F., Guo J., Wang W., Li G., Wang B., *Microgrid's multi-VSGs cooperative control method based on distributed communication*, Energy Reports, vol. 8, supplement 5, pp. 384–392 (2022), DOI: 10.1016/j.egyr.2022.02.191.

[11] Chen S., Sun Y., Han H., Luo Z., Shi G., Yuan L., Guerrero J.M., *Active power oscillation suppression and dynamic performance improvement for multi-VSG grids based on consensus control via COI frequency*, International Journal of Electrical Power & Energy System, vol. 147, 108796 (2023), DOI: 10.1016/j.ijepes.2022.108796.

[12] Li L., Sun Y., Liu Y., Tian P., Shen S., *A communication-free adaptive virtual inertia control of cascaded-type VSGs for power oscillation suppression*, International Journal of Electrical Power & Energy Systems, vol. 149, 109034 (2023), DOI: 10.1016/j.ijepes.2023.109034.

[13] Lin J., Liu S., Tian M., Huang M., Wang G., *Power oscillation suppression of multi-VSG based on both consensus and model predictive control*, International Journal of Electrical Power & Energy Systems, 109459 (2023), DOI: 10.1016/j.ijepes.2023.109459.

[14] Dattaa D., Sarker S.K., Rafiqul Islam Sheikh Md., *Designing a unified damping and cross-coupling rejection controller for LCL filtered PV-based islanded microgrids*, Engineering Science and Technology, International Journal, vol. 35, 101244 (2022), DOI: 10.1016/j.jestch.2022.101244.

[15] Ben Saïd-Romdhane M., Naouar M.W., Belkhodja I.S., Monmasson E., *Simple and systematic LCL filter design for three-phase grid-connected power converters*, Mathematics and Computers in Simulation, vol. 130, pp. 181–193 (2016), DOI: 10.1016/j.matcom.2015.09.011.

[16] Rashid T.H.M.S., Routh A.K., Rana M.R., Ferdous A.H.M.I., Sayed R., *A Novel Approach to Maximize Performance and Reliability of PMSG Based Wind Turbine: Bangladesh Perspective*, American Journal of Engineering Research (AJER), e-ISSN: 2320-0847, p-ISSN: 2320-0936, vol. 7, iss. 6, pp. 17–26 (2018).

[17] Camara M.S., Camara M.B., Dakyo B., Gualous H., *Modélisation et commande d'une génératrice synchrone à aimant permanant pour la production et l'injection des énergies offshores dans un réseau*, Symposium de Génie Électrique 2014, Cachan, France (2014).

[18] Dali A., Abdelmalek S., Bakdi A., Bettayeb M., *A new robust control scheme: Application for MPP tracking of a PMSG-based variable-speed wind turbine*, Renewable Energy, vol. 172, pp. 1021–1034 (2021) DOI: 10.1016/j.renene.2021.03.083.

[19] El Maataoui W., El Daoudi S., Lazrak L., Mabrouki M., *Minimized total harmonic distortion of a multi-level inverter of a wind power conversion chain synchronized to the grid-LCL filter optimization and third harmonic cancellation*, Electrica, vol. 22, no.°1, pp. 27–40 (2022) DOI: 10.5152/electrica.2021.21086.

[20] El Maataoui W., El Daoudi S., Lazrak L., Mabrouki M., *Improved Performance of the Grid Side Power Conversion Chain by Adopting Multilevel Inverter Topologies with an Optimized LCL Filter*, In: Motahhir S., Bossoufi B., (eds) Digital Technologies and Applications, ICDTA 2022, Lecture Notes in Networks and Systems, Springer, Cham, vol. 455 (2022), DOI: 10.1007/978-3-031-02447-4_52.

[21] Yan T., Wang C., Liu Z., Xu S., Ba Y., Fei J., Lin J.Y.S., *Research on pre-synchronization control strategy of the micro-grid with multi-VSG*, Global Energy Interconnection, vol. 1, iss. 3, pp. 376–381 (2018), DOI: 10.14171/j.2096-5117.gei.2018.03.009.

[22] Xiong K., Hu W., Zhang G., Zhang Z., Chen Z., *Deep reinforcement learning based parameter self-tuning control strategy for VSG*, Energy Reports, vol. 8, supplement 5, pp. 219–226 (2022), DOI: 10.1016/j.egyr.2022.02.147.

[23] Wu H., Ruan X., Yang D., Chen X., Zhao W., Lv Z., Zhong Q.C., *Small-Signal Modeling and Parameters Design for Virtual Synchronous Generators*, IEEE Transactions on Industrial Electronics, vol. 63, no. 7, pp. 4292–4303 (2016), DOI: 10.1109/TIE.2016.2543181.

[24] Liu J., Rafi F., Lu J., Hossain M.J., *Neutral Current Compensation in a VSG-Based Three-Phase Four-Wire Microgrid System*, IEEE International Conference on Environment and Electrical Engineering and 2018 IEEE Industrial and Commercial Power Systems Europe (EEEIC/I&CPS Europe), Palermo, Italy, pp. 1–6 (2018), DOI: 10.1109/EEEIC.2018.8494488.

[25] Wang D., Wu H., *Application of Virtual Synchronous Generator Technology in Microgrid*, IEEE 8th International Power Electronics and Motion Control Conference (IPEMC-ECCE Asia), Hefei, pp. 3142–3148 (2016), DOI: 10.1109/IPEMC.2016.7512798.

[26] Ur Rehman H., Yan X., Abdelbaky M.A., Ullah Jan M., Iqbal S., *An advanced virtual synchronous generator control technique for frequency regulation of grid-connected PV system*, International Journal of Electrical Power & Energy Systems, vol. 125, 106440 (2021), DOI: 10.1016/j.ijepes.2020.106440.

[27] Li S., Haskew T.A., Swatloski R.P., Gathings W., *Optimal and Direct-Current Vector Control of Direct-Driven PMSG Wind Turbines*, IEEE Transactions on Power Electronics, vol. 27, iss. 5, pp. 2325–2337 (2012), DOI: 10.1109/TPEL.2011.2174254.